Vibrational modes in the athermally photoinduced fluidity regime of glassy As_2S_3

D. Th. Kastrissios and G. N. Papatheodorou
Foundation for Research and Technology Hellas–Institute of Chemical Engineering and High Temperature Chemical Processes, P.O. Box 1414, GR-26500 Patras, Greece
and Department of Chemical Engineering, University of Patras, GR-26500 Patras, Greece

S. N. Yannopoulos*
Foundation for Research and Technology Hellas–Institute of Chemical Engineering and High Temperature Chemical Processes, P.O. Box 1414, GR-26500 Patras, Greece

(Received 5 February 2001; revised manuscript received 4 May 2001; published 1 November 2001)

A subbandgap light scattering investigation of vitreous arsenic trisulfide, v-As_2S_3, fibers subjected to external elongation stress has been undertaken in order to elucidate the photoinduced fluidity effect [H. Hisakuni and K. Tanaka, Science 270, 974 (1995)] in a microscopic scale. Orientational changes in the short-range order (intramolecular vibrations) caused by the presence of the illuminating visible light are detected. Subtle but noteworthy alterations are revealed in the intermediate range order, manifested as the increase of the magnitude and the modification of the frequency dependence of the depolarization ratio—in the low frequency part of the spectrum—as a function of the applied stress. The results are discussed alongside with old and recent structural models that have been employed to account for light-induced changes in amorphous semiconductors and low-energy modes in amorphous solids.

DOI: 10.1103/PhysRevB.64.214203 PACS number(s): 61.43.Dq, 42.70.Gi, 63.50.+x, 78.30.Fs

I. INTRODUCTION

The illumination of amorphous chalcogenide semiconductors with light having energy close or even lower than that of the bandgap of the material brings structural, mechanical, optical etc. changes on these materials. Such changes have been the subject of extensive investigations during the past two decades.[1,2] The changes are caused eventually by the creation of electron-hole pairs, after illumination, where their subsequent separation or recombination can enhance the electrical response or lead to the mentioned changes, respectively. In particular the nonradiative recombination may lead to structural rearrangements in the local (intramolecular) or the medium (intermolecular) range order; such rearrangements are ultimately responsible for the photoinduced phenomena mentioned above.

A number of the most thoroughly studied photoinduced effects comprise the reversible photodarkening[1] (redshift in the optical absorption edge), the photoinduced anisotropy[3] (including photoinduced birefringence and photoinduced dichroism), the giant photoexpansion[4] (volume changes up to 5% have been measured after exposition to light), athermal photomelting[5] (at low temperature ~77 K), etc. Mechanical or rheological changes have also been observed (decrease of the glass transition temperature T_g) and softening of the elastic constants under illumination.[1] Such photoinduced changes, related to the fluidity of amorphous As_2S_3 fibers subjected to elongation stress, have recently been revealed by Hisakuni and Tanaka, albeit without elucidating the microscopic origin of the effect.[6] In this work we have undertaken a light scattering (Raman) investigation attempting to clarify the changes brought about in both the disorder-induced scattering mechanism and the localized vibrational modes during the photoinduced fluidity effect.

The paper is organized as follows. In Sec. II we briefly outline the nature of photoinduced fluidity effect and the literature appeared so far aimed at its explanation. In Sec. III the experimental procedure (fiber preparation and light scattering apparatus) followed in this work is described. Section IV contains a short survey on the structural characterization of amorphous arsenic sulfide and a short background on disorder-induced scattering from amorphous solids and its interrelation to the intermediate range order. In Sec. V we present our results and attempt to unravel the specific photoinduced structural rearrangements through characteristic changes in internal vibrational modes and the low-energy vibrations of the medium. Section VI is devoted to a short description of structural models relevant to the microscopic origin of the photoinduced fluidity effect. Finally, Sec. VII contains the most important conclusions that can be drawn from the present study.

II. PHOTOINDUCED FLUIDITY

Hisakuni and Tanaka have demonstrated that the fluid state of a glassy semiconductor can be obtained by a process that does not require heat supply.[6] A local increase of the network fluidity emerges as a result of light illumination and can be revealed through the application of external stress. Specifically, the consequence of laser light (6328 Å) irradiation was the facilitation of viscous flow reducing the viscosity by more than two orders of magnitude. In other words, the equiviscous ($\eta \approx 2\times10^{12}$ poise) temperatures T' (without illumination) and T'' (under illumination) present a difference $T'-T'' \approx 200$ K. The effect becomes also macroscopically evident as an increasing elongation of a fiber's length under light illumination, manifested as a ''necking'' effect on the illuminated point. Quite interesting is the fact that the viscosity of the illuminated sample unexpectedly increases at higher temperatures. This fact indicated that the

photoinduced fluidity is not the effect of temperature rise because then the opposite behavior would be observed; namely, decreasing viscosity with increasing temperature.

A possible explanation for the aforementioned temperature dependence for the viscosity has been attempted by the authors[6] employing the concept of photoelectronic process. This relies on the well-known fact that illumination of chalcogenide glasses can produce electrons and holes where their recombination results to restructuring of atomic bonds. The specific mechanism however on the atomic scale is still hypothetical. It has been claimed that intramolecular and/or intermolecular bond changes may be responsible for the observed phenomenon. Further, Fritzsche[7] has attempted a rationalization of the athermal fluidity effect by employing the shelf-trapped exciton idea. In that sense, the photoexcited electron-hole pairs may recombine nonradiatively through passing from a transient exciton state. The final recombination may yield a bonding arrangement different from the initial configuration. According to this model[7] the observed macroscopic changes in the fluidity are the cumulative effect of the local configuration changes. In a more recent approach, first-principles molecular dynamics simulations have been utilized to calculate light-induced structural changes and diffusive motion in As_2S_3.[8] It has been observed, by calculating the system-average mean-squared variation in atomic position, that diffusive motion occurs for short times and this was interpreted as the initial stage of the athermal photoinduced fluidity.[8]

The elucidation of the structural mechanisms responsible for the observed photoinduced phenomena can be accomplished if certain spectral features revealed by particular experimental techniques can be attributed to specific atomic rearrangements. In that sense, Raman spectroscopy is a suitable probe that when applied in a condensed phase can furnish information concerning the local and the ''extended'' local structure. This is possible because internal vibrational modes are characteristic of the short-range order of the medium,[1] while low energy excitations in amorphous structures, probed by low frequency Raman studies, are usually considered as manifestations of the intermediate range order and/or as signatures of collective behavior.[9–11] It is therefore feasible, by using Raman spectroscopy, to track both intramolecular and intermolecular degrees of freedom and to monitor specific effects of photostructural changes on them. A preliminary account on a Raman spectroscopic study of amorphous As_2S_3 fibers under elongation stress can be found elsewhere.[12]

III. EXPERIMENT

Amorphous bulk quantities of As_2S_3, kindly provided by Professor H. Fritzsche, were used as the starting material. Proper bulk amount of the material (~5 gr) was placed in cylindrical fused silica tubes (o.d.=13 mm, i.d. 10 mm) that were filled with Ar gas after evacuation. Then the material was heated for homogenization at a temperature (~600 °C) far above the melting point of the corresponding crystal for 1–2 h. Homogeneous thin amorphous fibers with variable diameters were produced after immersing and extracting

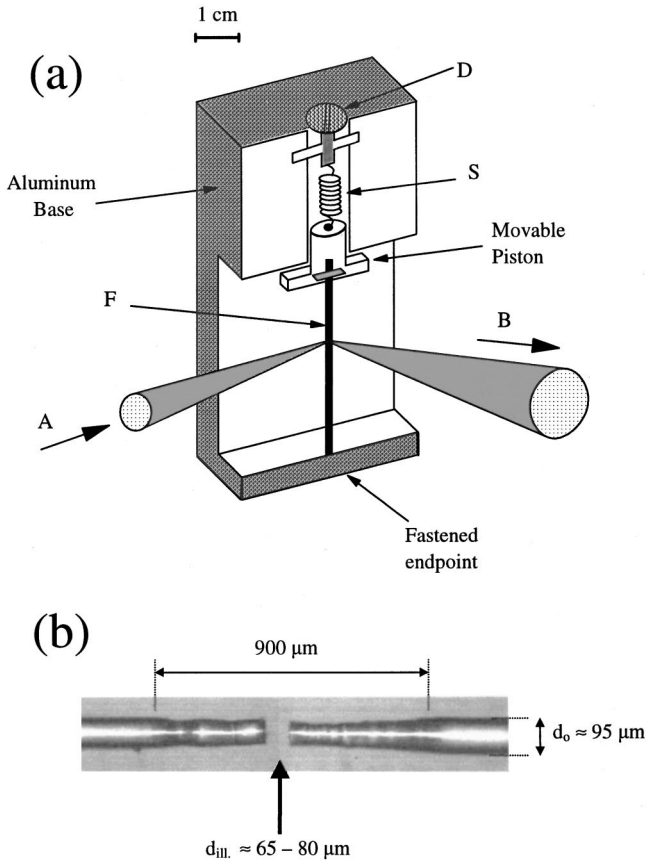

FIG. 1. (a) Schematic representation of the stretching device. *A*: incident beam; *B*: scattered light; *F*: v-As_2S_3 fiber; *S*: spring that provides the applied stress; *D*: calibrated screw. (b) v-As_2S_3 fiber, $d \approx 95\ \mu$m after light irradiation under longitudinal stretching.

with high speed a needlelike glassy (silica) rod in the melt. The speed of extraction of the fine object was to some extent determining the diameter of the produced fiber. The diameters of the fibers were measured through an optical microscope. Typical diameter magnitudes were found within 80–280 μm.

The stretching device, constructed in our machine shop, is schematically illustrated in Fig. 1(a). One of the fiber's end points is fastened on a stable block and the other one was attached to a moving support driven by the spring. The elongation of the latter and hence the applied force was determined by the proper rotation of a calibrated screw. The force constant of the spring has been determined by attaching to it known weights. During the fiber stretching the spring was loaded only within the elastic regime where the Hookean behavior is fulfilled. Figure 1(b) shows the permanent changes brought about to a fiber as the combined effect of light illumination and stress application.

Right-angle Raman spectra were recorded by a 0.85 m double monochromator (Spex 1403). The excitation source was a Kr^+ laser (Spectra Physics, model 2017) operating at the 647.1 nm (~1.92 eV) line with a power density on the sample ~10 W cm^{-2}. This low value of the incident radiation was used to match the conditions of the Hisakuni and Tanaka experiment avoiding thus to heat the sample with the

laser. The instrumental resolution was fixed at 1.5 cm^{-1} for the whole set of measurements performed at ambient temperature. Both scattering geometries, VV and HV, were employed. The signal after its detection from a water-cooled photomultiplier and its amplification from standard electronic equipment was transferred to a computer.

IV. BACKGROUND

A. Amorphous As_2S_3: Structure

A long body of experimental data, including x-ray and neutron diffraction, vibrational spectroscopy, viscosity and nuclear quadrupole resonance, suggest that glassy arsenic sulfide has a layeredlike structure.[13] Raman spectra of glassy arsenic trisulfide and especially the measured depolarization spectrum[14] have been shown to provide evidence in favor of the ''molecular model'' proposed by Lucovsky and Martin.[15] The molecular model associates bands in the spectra of glassy As_2S_3 with interpyramidal molecular vibrations between AsS_3 pyramidal units and intrapyramidal vibrations within an AsS_3 pyramidal unit. Interpyramidal vibrations are mostly identified with the deformation of the As-S-As ''waterlike'' angle. The AsS_3 pyramid and the bridging As-S-As modes are treated independently after the assumption that the intermolecular coupling is sufficiently weak.

B. Low energy excitations in amorphous solids

During the past two decades vivid interest has appeared concerning the study of the low-frequency features of amorphous solids and supercooled liquids from both experimental and theoretical point of view. Extra spectral features, in comparison with the corresponding crystal, appear universally for all glasses that are caused due to the disorder through the breaking down of the scattering wave vector conservation rule. Therefore, each mode in the system couples to the radiation, giving rise to a broad spectrum.

It has been early recognized that the low frequency Raman spectrum consists of two main contributions: the quasielastic component and the boson peak.[16] The quasielastic scattering is considered to arise from the interaction of light with fast (sub-picosecond) relaxators or from multiphonon scattering processes. It appears as a central mode ($\omega=0$) represented usually by a Lorentzian line with a half-width of the order 10–15 cm^{-1}. The boson peak is an asymmetrical vibrational feature with its maximum located in the interval 10–70 cm^{-1} and a high frequency tail extending up to 50–150 cm^{-1} depending on the material. The spectral features of this mode, i.e., shape, intensity, and polarization properties, have not been yet described rigorously by any theory on a satisfactory level. The reason is that for such an evaluation the knowledge of the microscopic mechanism that is responsible for the atomic polarizability modulation and the implications of structural disorder are needed but not yet known. The origin of the boson peak is not yet adequately understood but it is widely invoked the concept of medium range order and the collective character that this structural feature reflects.[11]

It has been recently argued that the Boson peak in layered glasses is a manifestation of the interlayer vibrations.[10] Therefore, opticlike motions of large non-bonded covalent structures against each other seems highly likely to be involved in the excess light scattered intensity around 24 cm^{-1}. This argumentation is also supported by the finding that although the high frequency vibrational spectra of As_2O_3 and As_2S_3 seem to coincide after scaling the frequency axis with the $\sqrt{m_{\text{oxygen}}/m_{\text{sulfur}}}$ ratio, the boson peak maxima are located at the same frequency for both glasses, i.e., $\sim$24 cm^{-1} at room temperature.

V. RESULTS AND DISCUSSION

A. Intramolecular vibrational modes: Local structure

Representative polarized and depolarized Stokes-side Raman spectra corresponding to the different magnitudes of the applied stress are shown in Fig. 2 for a fiber with diameter $d=225\ \mu$m. Dashed lines represent the isotropic part of the spectrum calculated through the relation $I^{\text{ISO}}=I^{\text{VV}}-(4/3)I^{\text{HV}}$, which is plotted together with the polarized and depolarized spectra to emphasize the relative changes that these spectra reveal. Indeed, drastic modifications are observed in the region 260–430 cm^{-1} where according to the ''molecular model'' analysis (see Sec. IV) three vibrational modes can be identified. Specifically the v_1 and v_3 vibrational modes of the C_{3v} symmetry AsS_3 pyramidal unit at 342 and 310 cm^{-1}, respectively, and the v_3' vibrational mode of the C_{2v} symmetry As-S-As waterlike unit at 392 cm^{-1}. The increase of the magnitude of the applied external stress causes a monotonic increase of the depolarization ratio $\rho(\omega)=I^{\text{HV}}/I^{\text{VV}}$ in the whole range of the spectrum which is better discernible in the region 260–430 cm^{-1}.

In order to distinguish between the changes brought about from the incident photon energy and the application of the stress itself we have undertaken a time dependent study of the Raman spectra of an illuminated fiber that was not subjected to elongation stress. The results have shown that no detectable changes are discernible from the measured spectra and the depolarization ratio remains constant independent of the exposure time, which was up to several hours. This implies that the modifications of the depolarization ratio are due to the combined effect of illumination and the application of the external stress, where the latter facilitates structural reorganization. The above findings provide an indirect proof of the link between changes in the depolarization ratio and the photoinduced fluidity effect.

To follow the stress dependence of the depolarization ratio in a quantified way we have conducted fits with Gaussian lines to the experimental spectra in the 260–430 cm^{-1} region. Representative fits are depicted in Fig. 3 for the bulk glass and for a fiber under elongation stress. An important outcome of this analysis is that the widths as well as the positions of the three peaks were found to be essentially stress-independent corroborating the perception that the applied stress has no effect on the bond lengths and the angles bridging the structural units. Alternatively, as will become clear later on, the elongation stress is most probably relieved

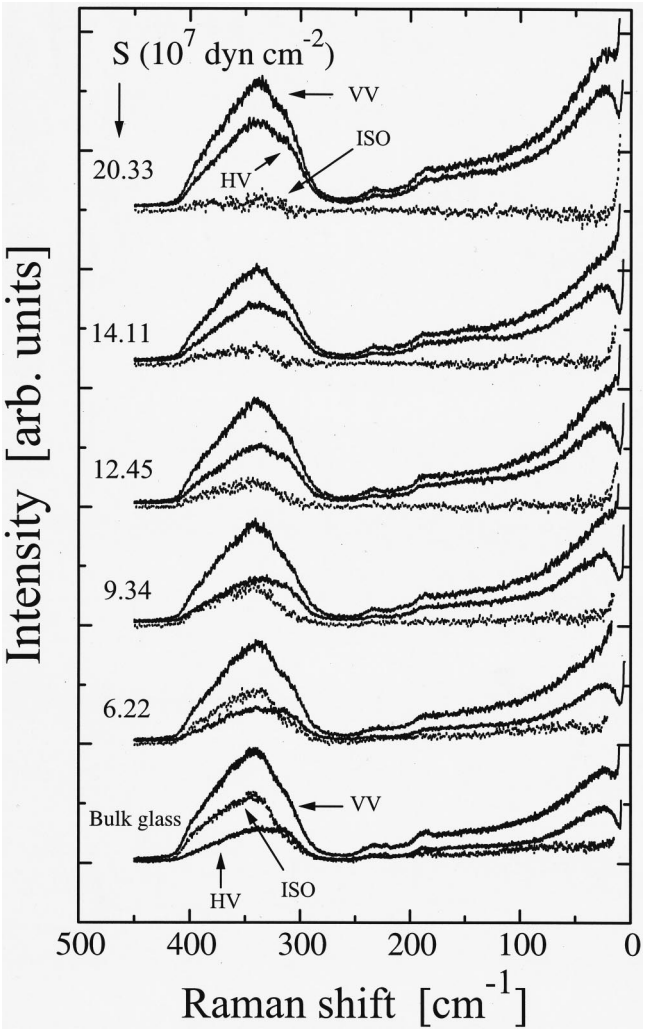

FIG. 2. Stokes-side Raman spectra of v-As_2S_3 fiber, $d \approx 225\ \mu$m under elongated stress. The dotted line corresponds to the isotropic part of the spectrum that has included in the figure to show better the rapid increase of the depolarized scattering with increasing external stress. Numbers besides the spectra denote the externally applied stress in units of 10^7 dyn cm^{-2}.

by the mutual slipping between layerlike clusters of the amorphous medium and hence micro-ordering effects have to be invoked to rationalize the depolarization ratio dependence on the stress. This argument is also supported by the result of the unstressed fiber experiment mentioned above.

The stress dependence of the depolarization ratio (area ratio) for the individual vibrational modes corresponding to the fitted peaks is depicted in Fig. 4 for various fiber diameters. It is seen that $\rho(\omega)$ follows a sigmoid increase leading eventually to saturation at the highest magnitudes of the applied stress. This saturation may imply the consumption of the ''entities'' responsible for the facilitation of photoflow. Such saturation behavior is usually observed in many other photoinduced phenomena.[1]

A related publication has recently appeared wherein the effect of subbandgap light illumination on the time dependence of the Raman spectra depolarization ratio for various As_xS_{1-x} glasses is reported.[17] In that work, the depolarization ratio above 250 cm^{-1} was found time-independent while in the frequency range 80–250 cm^{-1} the depolarization ratio experiences a significant dependence on time. This result seems at a first glance surprising for the reason that the spectra at both frequency regions originate from bond-stretching and bond-bending vibrational modes and not from intermediate or mesoscopic vibrational excitations as the authors suggest for the 80–250 cm^{-1} region. Specifically, according to Ref. 15 the following assignment has been given: at 133 and 162 cm^{-1} are located the v_4 and v_2 vibrational modes of the C_{3v} symmetry for the AsS_3 pyramidal unit, while the peak at 218 cm^{-1} is associated with the v_1' vibrational mode of the C_{2v} symmetry for waterlike unit As-S-As. Further, it is well known that the mesoscopic vibrational excitations give rise to the lowest observed modes, e.g., the boson peak.[10,11] Our time dependent time data for As_2S_3 fibers, as mentioned above, in the absence of stress do not reveal changes similar to those reported in Ref. 17.

B. Low-energy excitations: Intermediate range structure

As it has been pointed out in Sec. IV the frequency of the boson peak maximum, $\Omega_{\max}^{BP}$, may be used as an indicator of subtle structural changes that take place in an intermediate length scale during the photoinduced fluidity effect. It is plausibly expected that such changes for $\Omega_{\max}^{BP}$ could be modest and a quantitative treatment (fitting) of the spectrum is necessary to detect them. A formal basis to carry out such a fitting procedure, that is relatively simple and does not involve a large number of parameters and approximations, is

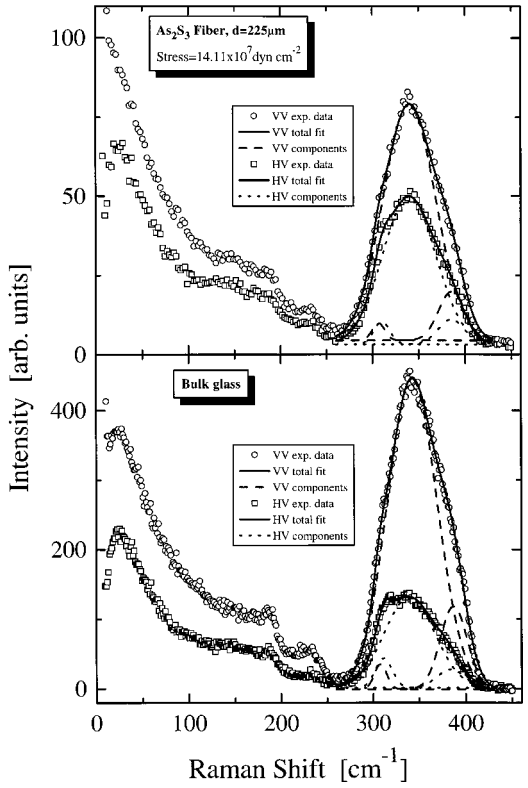

FIG. 3. Representative fits of the high-frequency Raman spectra with the three-Gaussians model. Solid lines represent the total fitted curves while long- and short-dashed lines represent the individual vibrational components as described in the text.

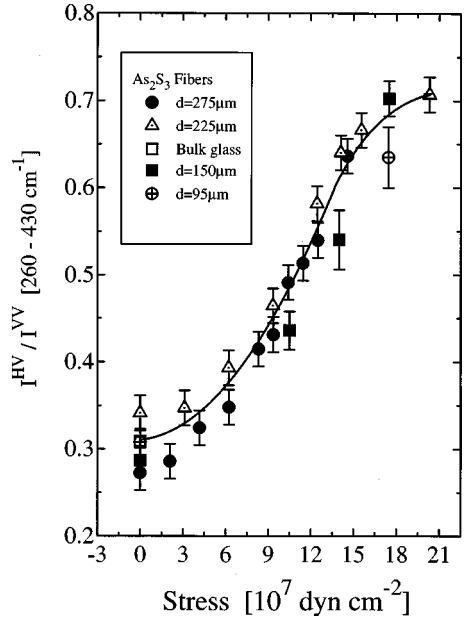

FIG. 4. External stress dependence of the depolarization ratio in the high-frequency region 260–340 cm^{-1} for various fibers diameters as indicated in the legend. The solid line is used as a guide to the eye.

the log-normal model (for details, see Ref. 18). The final fitting expression employed in our analysis is a composite model consisting of the sum of a Lorenztian line, used to account for the quasielastic or relaxational contribution centered at zero frequency, and the log-normal distribution for the reduced form of the boson peak,

$$I^R(\omega)=\frac{I_0}{\sqrt{2\pi}\sigma}\exp\left(-\frac{(\ln\omega-\ln\Omega_{\max}^{\mathrm{BP}})^2}{2\sigma^2}\right). \qquad (1)$$

I_0 is an arbitrary intensity prefactor and σ the half-width of the log-normal distribution. The reduction scheme followed here is that originally introduced by Shuker and Gammon,[19] e.g., $I^R(\omega)=I^{\exp}(\omega)/\omega[n(\omega,T)+1]=\omega^{-2}C(\omega)g(\omega)$, where $I^{\exp}(\omega)$ is the intensity of the Stokes Raman spectrum, $C(\omega)$ is the photon-phonon coupling coefficient, $g(\omega)$ represents the vibrational density of states, and $n(\omega,T)=[\exp(\hbar\omega/k_BT)-1]^{-1}$ is the Bose occupation factor.

In Fig. 5 we present the analysis of the low frequency data by means of the model that we have described above. The total fitted curve (continuous line) conforms almost perfectly to the experimental data (open circles) for the whole frequency range. It is clearly seen that the position of the maximum of the boson peak is located at the same frequency for the bulk glass and the fiber under any loaded stress. The insensitivity of both the $\Omega_{\max}^{\mathrm{BP}}$ and the spectral shape of the boson peak on the external stress implies that structural changes brought about during the effect do not involve changes in the size distribution of the layerlike clusters. Further, it would be instructive to monitor the behavior of the frequency dependence of the depolarization ratio in the region of the boson peak. This has been determined and illustrated in Fig. 6. We would like to stress again here that the frequency dependence of the depolarization ratio is a much more sensitive indicator for sensing possible changes of a scattering mechanism.

Two main observations come out from Fig. 6. First, the depolarization ratio increases when intensifying the external stress with a rate similar to that of the internal vibrational modes. Second, while a clear frequency dependence can be definitely evidenced in the depolarization ratio of the bulk glass and the unstressed (or slightly stressed) fiber this dependence is gradually smoothed out leading finally to a constant $\rho(\omega)$ for the highest applied stress values. This significant feature revealed by the depolarization ratio indicates a change in the scattering mechanisms that contribute in the frequency range 20–100 cm^{-1} while the fairly insensitive position of the boson peak maximum implies no change in the correlation length $R_c\propto v_s/\Omega_{\max}^{\mathrm{BP}}$ (v_s is a mean sound velocity) associated with structural disorder. It should be kept in mind that the photon-phonon coupling coefficient $C(\omega)$ is the only one quantity contributing to the Raman spectrum that carries polarization information. Then we are led to the conclusion that the observed changes depicted in Fig. 6 are reflected on changes of the coupling coefficient and in turn on the atomic polarizability modulation since by definition[19]

$$C^{\alpha\beta}(\omega)\propto FT\left\langle\frac{\partial\varepsilon_\alpha(\mathbf{r}')}{\partial Q_j}\frac{\partial\varepsilon_\beta(\mathbf{r}'+\mathbf{r})}{\partial Q_j}\right\rangle, \qquad (2)$$

where $\partial\varepsilon/\partial Q_j$ represents the strength of the polarizability modulation of the normal mode j; the different components

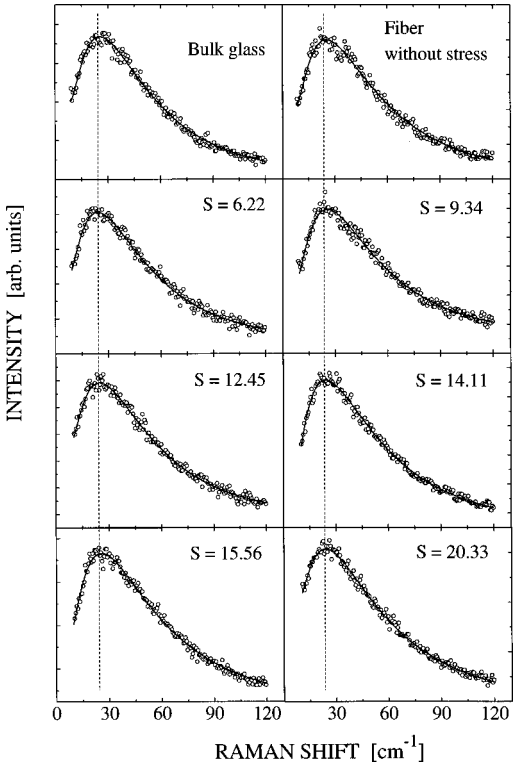

FIG. 5. Boson peak part of the Raman spectra fitted with the superposition model, Eq. (1) and a zero centered Lorentzian line to account for the quasielastic scattering. The low-frequency Raman spectrum of the bulk glass is also included to allow direct comparison among the various spectra.

labeled $\alpha\beta$ denote particular polarization geometries, and FT denotes Fourier transform. Recently, experimental evidence has been provided for the frequency dependence of the depolarization ratio for many inorganic glasses and the weakness of the approaches that determine the frequency dependence of the $C(\omega)$ by a direct comparison of neutron and light scattering data without taking into account the fact that the coupling coefficient exhibits polarization-dependent frequency behavior has been discussed.[20,21]

For a quantitative description of the stress dependent polarization properties of $C(\omega)$ we have attempted to model the frequency dependence of the depolarization ratio spectra with a power law of the form

$$\rho(\omega) \propto \omega^{\alpha(S)}, \tag{3}$$

where $\alpha(S)$ is a stress-dependent exponent. Figure 7 shows the stress dependence of the $\alpha(S)$ exponent and the inset shows a representative fit of the depolarization ratio spectrum for the bulk glass using Eq. (3). As is evident, the exponent $\alpha(S)$ presents a linear dependence on the applied stress reaching asymptotically the zero value that implies the loss of the frequency dependence for the coupling coefficient. The exponent $\alpha(S)$, in the linear regime, can be described as $\alpha(S) = -0.27 + 0.016S$. The ω independence reached eventually after ''stretching'' the structure to the highest possible extent may suggest that the scattering mechanisms involved in the 20–80 cm^{-1} region become

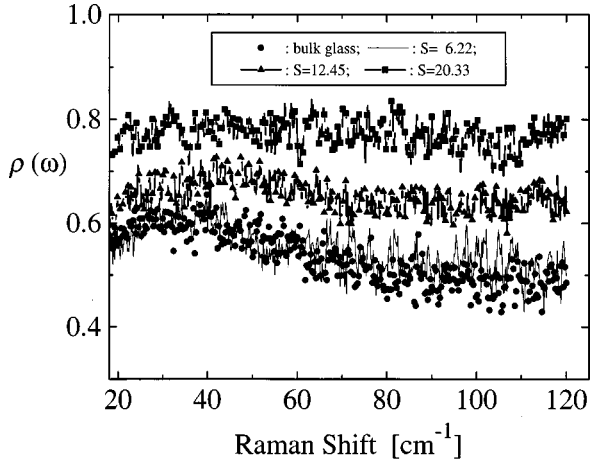

FIG. 6. External stress dependence of the depolarization ratio spectra in the low-frequency Raman region. Apart from an overall increase, a continuously changing slope can be observed as the magnitude of the stress increases.

gradually coupled as the stress increases. This could be interpreted from the point of view that both isotropic and anisotropic vibrational motions modulate the polarizability of the medium in a similar way.

Due to the complicated nature of the coupling coefficient as can be seen from Eq. (2) there are only few theoretical approaches so far aiming to address its frequency dependence; one that is more frequently used is that employing fractal concepts.[22] Tests of such theories have been performed in cases where the average coordination number in ideal covalent networks is systematically changed, e.g., see Ref. 23. It would be also interesting to check here the case where the structure is not chemically modified but mechanically reformed.

The vibrational density of states of fractons (vibrational excitations in fractal structures) that exist above a crossover frequency ω_ξ follows the power law form $g(\omega) \propto \omega^{\tilde{d}-1}$,[24] where $\tilde{d} = 4/3$. The light scattering susceptibility has been shown to read as[25]

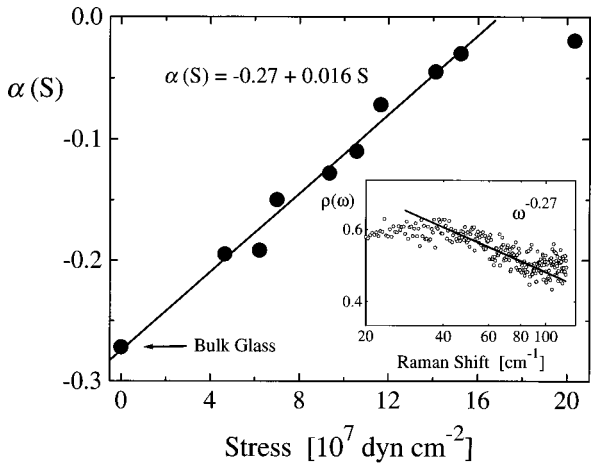

FIG. 7. External stress dependence of the power law exponent after fitting the depolarization ratio spectra with Eq. (3).

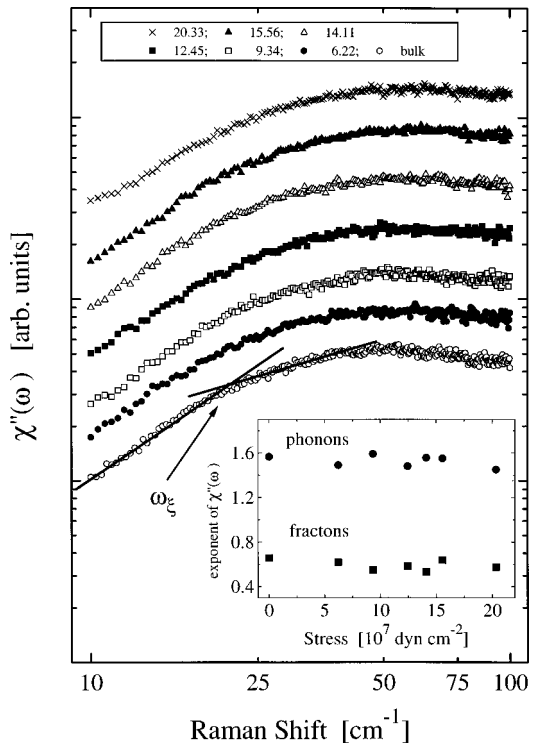

FIG. 8. Susceptibility representation of the low-frequency Raman spectra in double logarithmic plot. The power law fits to the fraction ($\omega<\omega_\xi$) and the phonon ($\omega>\omega_\xi$) regime with Eq. (4) are shown only in the bulk glass spectrum for simplicity. The power law exponents are plotted in the inset as a function of the applied stress.

$$\chi''(\omega)\equiv\frac{I^{\exp}(\omega)}{n(\omega)+1}\propto\omega^{(2\tilde{d}/D_f)+\tilde{d}-2}. \tag{4}$$

Therefore, the photon-phonon coupling coefficient in the fracton regime can be qualitatively obtained as

$$C(\omega)\propto\omega^{2\tilde{d}/D_f}. \tag{5}$$

Applying the mentioned ansatz to our low-frequency Raman spectra and plotting the susceptibility in Fig. 8 the following observations can be made. (i) The crossover frequency ω_ξ that separates the phonon ($\omega<\omega_\xi$) from the fracton ($\omega>\omega_\xi$) regime is located close to the boson peak maximum, e.g., at about 24 cm^{-1} and seems to be almost stress-independent. (ii) Two frequency regimes, obeying different power law dependence, are revealed from the spectra, namely region [I]:$10<\omega<20\,cm^{-1}$ and region [II]:$30<\omega<50\,cm^{-1}$ with almost stress independent exponents; see inset and mean values 1.53 and 0.59 for regions [I] and [II], respectively. In the phonon regime, where the Debye form for $g(\omega)$ is reasonable, we obtain $C(\omega)\propto\omega^{0.53}$. These findings do not corroborate neither contradict the applicability of fractal models. However, the ω dependence of $\rho(\omega)$ reveals the necessity of introducing polarization dependent fractal exponents if Eq. (5) is to be valid. Fractal models do not so far account for such a behavior.

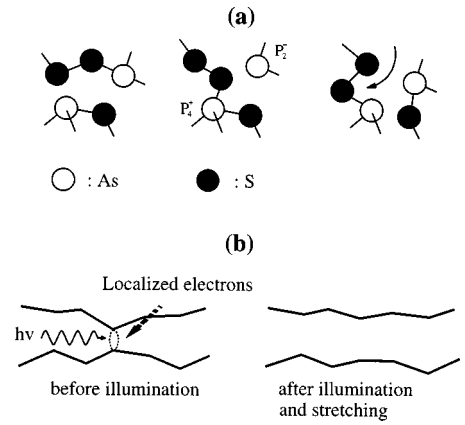

FIG. 9. Schematic representation of the two relevant microscopic models related to the photoinduced fluidity effect as described in the text; (a) self-trapped exciton, Ref. 7, and (b) buckling model, Ref. 26.

VI. TWO RELEVANT PICTURES FOR THE PHOTOINDUCED FLUIDITY

Let us now turn to the physical picture behind the results presented in the previous section. As has been already mentioned in Sec. II the self-trapped exciton model is a relevant microscopic description of photoinduced structural changes that involves certain modifications on an *intramolecular* basis; see Fig. 9(a). The formation of a transient state and its subsequent relaxation to a final configuration where bonds are arranged in a direction perpendicular to the initial one might reasonably well justify the changes observed in the polarization properties of the scattered light. Further, structural modifications on an *intermolecular* scale are also likely to happen.

A quite relevant picture, the buckling model, which invokes the layerlike properties of chalcogenide glasses, has been introduced some years ago by Ihm[26] to account for optical absorption tails of glasses. It has been proposed that the layerlike remnants (clusters) that exist in amorphous chalcogenides could be buckled at some particular atoms where electrons can be localized forming an additional weak interlayer bond. The electrons can become delocalized either by thermal activation (temperature rise) or by photoexcitation. Buckling removal may lead to a release of the excess strain and finally to an effective slipping between neighboring clusters, thus resulting in the observed increased fluidity and the macroscopic elongation of the fiber; see Fig. 9(b).

The adoption of the idea that the removal of the constraint brought about by the ''buckling atoms'' facilitates the athermal flow process seems also compatible with the results obtained by the examination of the low-frequency Raman spectra. Indeed, the established insensitivity of both the log-normal distribution width σ and the $\Omega_{\max}^{BP}$ on the applied stress forces us to envisage that breaking or disruption of the clusters seems highly unlikely to take place. The applied external stress can be relieved after annulling the buckling constraints and the undulated layerlike cluster may finally acquire a more ''flat'' structure. However, this modification on the configuration of the layers should affect the low-

energy excitations. This is eventually observed in the systematic stress dependent slope of the depolarization ratio; see Fig. 6.

We may also recall here the recently proposed ''slip and repulsion model'' that has been proposed to account for the photodarkening and photoinduced volume expansion in chalcogenide glasses.[27] In this model the layerlike structure is again the requisite for explaining the mentioned effects. Therefore, the volume expansion is the result of the electrostatic repulsion forces between adjacent layers. These forces are built up due to the different mobility of charge carriers, namely electrons and holes. Based on the slip and repulsion model we may conclude that if such an expansion mechanism takes place it should facilitate the mutual slipping of the layers after applying the external elongation stress.

VII. CONCLUDING REMARKS

A light scattering (Raman) study has been undertaken to elucidate the microscopic origin of the photoinduced fluidity effect. Investigation of both high-frequency vibrational modes (*intramolecular* degrees of freedom) and low-energy excitations (*intermolecular* degrees of freedom) has been attempted. In particular, a stress dependence study of the Raman spectra has been carried out for v-As_2S_3 fibers of different diameters. Systematic effects have been observed in the depolarization ratio spectra for the whole frequency region studied, which have been considered to reflect the structural changes occurring during the photoinduced fluidity effect. In particular the main conclusions drawn from the present work can be summarized as follows:

(i) The depolarization ratio in the high-frequency vibrations shows a monotonic increase presenting a sigmoid behavior. On the contrary, the peak positions and widths of the intramolecular vibrational modes do not exhibit any variations as a function of the applied stress. These findings imply that during illumination and stretching the structural modifications that take place do not involve substantial bond length and/or bond angle alterations. The observed behavior has to be seen rather as the result of micro-ordering effects brought about as the combined effect of irradiation and stretching the layerlike structure.

(ii) The analysis of the low-energy excitations has revealed similar trends in the depolarization ratio spectra. On the other hand, the position and the shape of the boson peak did not show any variation as a function of the externally applied longitudinal stress. Interestingly, the frequency dependence of $\rho(\omega)$ in the low-frequency region, apart from an overall increase, was found to exhibit also a significant stress dependence. This finding shows that the photon-phonon coupling coefficient, that accounts for the degree of the medium's polarizability modulation due to vibrational motion experiences significant changes. In particular, its polarized and depolarized components tend to assume the same frequency dependence as the magnitude of the applied stress increases. This fact has been interpreted as the result of layer structure ''flattening'' taking place after the removal of buckling constraints and/or local structure reorganization such as that described in the self-trapped exciton model.

(iii) The low-frequency modes have also been treated in the spirit of the fractonlike excitations in amorphous solids. The phonon to fracton crossover was found close to the Boson peak maximum and almost stress-independent. However, the analysis has revealed the inadequacy of such models, based on fractal concepts, to describe structure and dynamics in amorphous media in the case where the spectral form of the scattered light depends upon the employed polarization geometry.

Finally, some comments should be made concerning the glass transition dynamics in chalcogenide glasses. The facilitation of the network flow due to the combined effect of subbandgap light illumination and stretching is the outcome of certain structural rearrangements that are also expected to have important impact on the structural relaxation of the material. As has been already mentioned in Sec. II, rheological properties such as viscosity undergo changes that correspond to about 200 K temperature transformation. It seems therefore quite significant the fact that one can affect the dynamic properties of a material in a limited spatial region with a procedure characterized by the very local character of the interaction; an operation almost impossible to achieve with conventional thermal techniques. Therefore, work is currently in progress in order to clarify the distinct role of temperature and light illumination.

ACKNOWLEDGMENTS

S.N.Y. acknowledges financial support from the General Secretariat of Research and Technology–Hellas in the framework of the PENED/99EΔ44 grant. The authors wish to thank Prof. H. Fritzsche for pointing out the photoinduced fluidity effect and for providing As_2S_3.

*Author to whom correspondence should be addressed. Electronic address: sny@iceht.forth.gr

[1] For general reviews on the subject see, for example, K. Shimakawa, A. V. Kolobov, and S. R. Elliott, Adv. Phys. **44**, 475 (1995); A. V. Kolobov and K. Tanaka, in *Handbook of Advanced Electronic and Photonic Materials and Devices*, edited by H. S. Nalwa (Academic, New York, 2001), Vol. 5, p. 47.

[2] See, for example, *Proceedings of the 18th International Conference on Amorphous Semiconductors–Science and Technology (ICAMS)*, Snowbird, Utah [J. Non-Cryst Solids **266-269** (2000)].

[3] A. V. Kolobov, V. Lyubin, T. Yasuda, M. Klebanov, and K. Tanaka, Phys. Rev. B **55**, 8788 (1997); H. Fritzsche, *ibid.* **52**, 15 854 (1995).

[4] H. Hisakuni and K. Tanaka, Appl. Phys. Lett. **65**, 2925 (1994).

[5] V. V. Poborchii, A. V. Kolobov, and K. Tanaka, Appl. Phys. Lett. **74**, 215 (1999).

[6] H. Hisakuni and K. Tanaka, Science **270**, 974 (1995).

[7] H. Fritzsche, Solid State Commun. **99**, 153 (1996).

[8] J. Li and D. A. Drabold, Phys. Rev. Lett. **85**, 2785 (2000).

[9] A. P. Sokolov, A. Kisliuk, M. Soltwisch, and D. Quitmann, Phys.

Rev. Lett. **69**, 1540 (1992).
[10] S. N. Yannopoulos, G. N. Papatheodorou, and G. Fytas, J. Chem. Phys. **107**, 1341 (1997).
[11] S. R. Elliott, Europhys. Lett. **19**, 201 (1992).
[12] D. Th. Kastrissios, S. N. Yannopoulos, and G. N. Papatheodorou, Physica B **296**, 216 (2001).
[13] R. Zallen, *Physics of Amorphous Solids* (Wiley, New York, 1983); L. E. Busse, Phys. Rev. B **29**, 3639 (1984).
[14] R. J. Kobliska and S. A. Solin, Phys. Rev. B **2**, 756 (1972).
[15] G. Lucovsky and R. M. Martin, J. Non-Cryst. Solids **8-10**, 185 (1972).
[16] J. Jäckle, in *Amorphous Solids: Low-Temperature Properties*, edited by W. A. Phillips (Springer, Berlin, 1981), p. 135.
[17] K. Matsuishi, R. Arima, K. Kagota, and S. Onari, J. Non-Cryst. Solids **266-269**, 938 (2000).
[18] I. Pocsik and M. Koos, Solid State Commun. **74**, 1252 (1990); T. Pang, Phys. Rev. B **45**, 2490 (1992).
[19] R. Shuker and R. Gammon, Phys. Rev. Lett. **25**, 222 (1970).
[20] S. N. Yannopoulos and G. N. Papatheodorou, Phys. Rev. B **62**, 3728 (2000).
[21] S. N. Yannopoulos, J. Chem. Phys. **113**, 5868 (2000).
[22] For recent reviews on fractals aspects of amorphous media, see T. Nakayama, K. Yakubo, and R. Orbach, Rev. Mod. Phys. **66**, 381 (1994); *Fractals and Disordered Systems*, 2nd ed., edited by A. Bunde and S. Havlin (Springer-Verlag, Berlin, 1996).
[23] M. Nakamura, O. Matsuda, and K. Murase, Phys. Rev. B **57**, 10 228 (1998).
[24] S. Alexander and R. Orbach, J. Phys. (France) Lett. **43**, L625 (1982).
[25] E. Duval, G. Mariotto, M. Montagna, O. Pilla, G. Villiani, and M. Barland, Europhys. Lett. **3**, 333 (1987).
[26] J. Ihm, J. Phys. C **18**, 4741 (1985).
[27] K. Shimakawa, N. Yoshida, A. Ganjoo, Y. Kuzukawa, and J. Singh, Philos. Mag. Lett. **77**, 153 (1998).